Articles in PresS. J Neurophysiol (October 5, 2005). doi:10.1152/jn.00696.2005

LTP regulates burst initiation and frequency at mossy fiber – granule cell synapses of rat cerebellum: experimental observations and theoretical predictions

Thierry Nieus[1,2], Elisabetta Sola[1,4], Jonathan Mapelli[1], Elena Saftenku[3], Paola Rossi[1], Egidio D'Angelo[1,2,]*

[1] Dept. of Cellular-Molecular Physiological and Pharmacological Sciences (University of Pavia) and INFM, Via Forlanini 6, I-27100, Pavia, Italy.
[2] Dept. of Functional and Evolutionary Biology (University of Parma), Parco Area delle Scienze 11a, I-34100, Parma, Italy.
[3] Dept. of General Physiology of Nervous System, A.A. Bogomoletz Institute of Physiology Bogomoletz St., 4, 01024, Kiev-24, Ukraine
[4] present address: Dept. of Biophysics, SISSA, via Beirut 4, I-34014, Trieste, Italy

* To whom correspondence should be addressed at dangelo@unipv.it

Key-words. LTP, Synaptic plasticity, Presynaptic mechanisms, Cerebellum, Granule cells

Running title. LTP and bursting in the cerebellum

Acknowledgments. This work was supported by projects of the European Community (CEREBELLUM QLG3-CT-2001-02256 and SPIKEFORCE IST-2001-35271), of MIUR and INFM of Italy to ED.

ABSTRACT

Long-term potentiation (LTP) is a synaptic change supposed to provide the cellular basis for learning and memory in brain neuronal circuits. Although specific LTP expression mechanisms could be critical to determine the dynamics of repetitive neurotransmission, this important issue remained largely unexplored. In this paper we have performed whole-cell patch-clamp recordings of mossy fiber – granule cell LTP in acute rat cerebellar slices and investigated its computational implications with a mathematical model. During LTP, stimulation with short impulse trains at 100 Hz revealed earlier initiation of granule cell spike bursts and a smaller non-significant spike frequency increase. In voltage-clamp recordings, short AMPA EPSC trains showed short-term facilitation and depression and a sustained component probably generated by spillover. During LTP, facilitation disappeared, depression accelerated, and the sustained current increased. The NMDA current also increased. In agreement with a presynaptic expression due to increased release probability, similar changes were observed by raising extracellular [Ca^{2+}]. A mathematical model of

mossy fiber – granule cell neurotransmission showed that increasing release probability efficiently modulated the first-spike delay. Glutamate spillover, by causing tonic NMDA and AMPA receptor activation, accelerated EPSP temporal summation and maintained a sustained spike discharge. The effect of increasing neurotransmitter release could not be replicated by increasing receptor conductance, which, like postsynaptic manipulations enhancing intrinsic excitability, proved very effective in raising granule cell output frequency. Independent regulation of spike burst initiation and frequency during LTP may provide mechanisms for temporal re-coding and gain control of afferent signals at the input stage of cerebellar cortex.

INTRODUCTION

Brain neuronal circuits transmit signals often organized in spikes sequences, or bursts (Rieke et al. 1996; Lisman, 1997; Krahe and Gabbiani, 2004). Bursts can be processed by two forms of short-term synaptic plasticity, facilitation and depression, which reflect the dynamics of synaptic vesicle cycling and regulate EPSP temporal summation (O'Donovan and Rinzel, 1997; Buonomano, 2000). The time-dependent properties of the synapse could be changed by long-term synaptic plasticity (Tsodyks and Markram, 1997). Long-term potentiation or depression (LTP or LTD) can alter several functional aspects of the synapse, including neurotransmitter release, neurotransmitter spillover, and postsynaptic receptor gating and expression (Kullman et al., 1996; Malenka and Nicoll, 1999; Bliss et al, 2003; Lisman, 2003). Although the particular mechanism of expression could be critical to determine the consequences of LTP and LTD on repetitive neurotransmission at specific synapses, this important issue remained largely unexplored.

In this paper, instead of considering synaptic responses to isolated impulses, we have investigated the response to stimulus trains at the mossy fiber – granule cell relay of cerebellum. Mossy fiber activity *in vivo* is characterized by repetitive discharges (Kase et al., 1980; Chadderton et al., 2004). Investigations in acute cerebellar slices have revealed that repetitive stimulation causes depression in AMPA and summation in NMDA receptor-dependent responses (D'Angelo et al., 1995). The AMPA response includes a slow component determined by glutamate spillover, which also plays a major role in NMDA receptor activation (DiGregorio et al., 2002; Rossi et al., 2002; Cathala et al., 2003; Xu-Friedman and Regehr, 2003). Interestingly, mossy fiber – granule cell LTP induced by theta-burst stimulation is expressed presynaptically through an enhanced neurotransmitter release probability (Sola et al., 2004). Thus, the mossy fiber – granule cell relay of cerebellum provides the opportunity of investigating the relationship between synaptic mechanisms and the impact of LTP on neurotransmission dynamics.

In this paper we have investigated the effect of release probability changes on mossy fiber –

granule cell neurotransmission by combining patch-clamp recordings in cerebellar slices with mathematical modeling. LTP increased the first EPSC amplitude, accelerated short-term depression and, at the same time, enhanced sustained AMPA and NMDA receptor-mediated currents. As a result, granule cell discharge was initiated earlier while a sustained discharge frequency was maintained. Simulations showed that these effects required glutamate spillover in the cerebellar glomerulus and could not be replicated by postsynaptic changes in receptor conductance or intrinsic excitability, which preferentially modulated frequency rather than timing. Thus, the mossy fiber – granule cell relay, through a long-term control of pre- and postsynaptic mechanisms, can regulate the timing and frequency of input bursts. These mechanisms may have important consequences for the two main operations supposed to take place in the cerebellum granular layer, namely elaboration of temporal dynamics (Braitenberg, 1967; Medina and Mauk, 2000) and gain control (Albus, 1971; Mitchell and Silver, 2003).

METHODS

Patch-clamp recordings in acute cerebellar slices

Patch-clamp recordings in acute cerebellar slices were performed as previously reported (D'Angelo et al., 1995, 1999; Armano et al., 2000). Briefly, slices were cut in the sagittal plane from the cerebellar vermis of 18-to-23 day-old Wistar rats. Recording temperature was maintained at 30 °C with a feed-back Peltier device (TC-324B, Warner Instr. Corp., Hamden, CT, USA).

Krebs solution for slice cutting and recovery contained (mM): NaCl 120, KCl 2, $MgSO_4$ 1.2, $NaHCO_3$ 26, KH_2PO_4 1.2, $CaCl_2$ 2, glucose 11, and was equilibrated with 95% O_2 and 5% CO_2 (pH 7.4). Krebs solutions with different Ca^{2+} concentrations (from 1 mM to 4 mM) were prepared maintaining the total concentration of divalent cations constant by corresponding changes in Mg^{2+}. During recordings, the GABA-A receptor blocker, 10 μM bicuculline, was added to the solutions . Local drug perfusion was performed through a multi-barrel pipette. Perfusion with control extracellular solution was commenced before seal formation and was maintained until switching to the test solutions. The patch-clamp pipette solution for current-clamp recordings contained (mM): K-gluconate 126, NaCl 4, $MgSO_4$ 1, $CaCl_2$ 0.05, BAPTA 0.1, glucose 15, ATP-Mg 3, GTP 0.1, HEPES 5. This solution maintained resting free [Ca^{2+}] at 100 nM and pH was adjusted to 7.2 with KOH. Patch-clamp pipettes filled with this solution had a resistance of 5-8 MΩ before seal formation. The patch-clamp pipette solution for voltage-clamp recordings contained (mM): Cs_2SO_4 81, NaCl 4, $MgSO_4$ 2, $CaCl_2$ 0.05, BAPTA 0.1, glucose 15, ATP-Mg 3, GTP 0.1, HEPES 15. This solution maintained resting free [Ca^{2+}] at 100 nM and pH was adjusted to 7.2 with CsOH. Patch-clamp pipettes filled with this solution had a resistance of 3-5 MΩ before seal formation. All drugs

were obtained from Sigma, except BAPTA tetrapotassium salt (Molecular Probes, Eugene, OR, USA), D-2-amino-5-phosphonovaleric acid (APV), 7-Cl-kynurenic acid (7-Cl-Kyn) and 6-cyano-7-nitroquinoxalene-2,3-dione (CNQX) (Tocris-Cookson, Avonmouth, UK).

Recordings were performed with an Axopatch 200-B amplifier and signals sampled with a Labmaster 1200-B interface (sampling rate = 10 kHz). Current and voltage traces were digitally filtered at 3 kHz and analyzed off-line with P-Clamp (Axon Instruments) and Igor (Wavemetrics) software. Data are reported as mean ± SEM and, unless otherwise indicated, statistical comparisons are done using paired Student's *t*-test and differences are considered statistically not significant for $p>0.05$.

Mossy fibers were stimulated with a bipolar tungsten electrode or a patch-pipette via an isolation unit at a basal frequency of 0.33 Hz. In certain sets of recordings we used minimal stimulation which, as explained in Sola et al (2004), usually allows to activate single mossy fiber – granule cell synapses. Single fiber stimulation was useful to investigate synaptic dynamics, since these may differ from synapse to synapse. Moreover, single fiber stimulation allowed high resolution of EPSP temporal summation, which could be directly compared to voltage-clamp recordings and mathematical simulations. In different experiments, either regular or random trains of impulses were applied every 30 sec. Regular trains typically had frequencies of 50 Hz and 100 Hz. Random trains with average frequency of 50 Hz were extracted from a Poisson distribution. The trains, either regular or random, were repeated 20-50 times and averaged off-line to reduce quantal variability. Extinction of short term plasticity between trains was monitored by evoking EPSCs (or EPSPs) at 0.33 Hz. In current-clamp recordings, every 5 minutes a step current protocol was executed to monitor intrinsic excitability (Armano et al., 2000). LTP was induced by 8 bursts of 10 impulses at 100 Hz, which were repeated every 250 milliseconds (theta-burst stimulation, TBS). In current-clamp, induction was enhanced by slightly depolarizing membrane potential to allow reliable spike activation during trains. In voltage-clamp, during induction trains membrane potential was stepped to -30 mV.

In VC recordings at –70 mV, the fast component of mossy fiber – granule cell EPSCs is due to activation of AMPA receptors (Silver et al., 1996a,b; D'Angelo et al., 1999; see Fig. 3A), so that AMPA EPSC amplitude was measured as the difference between EPSC peak and the current level just before stimulation (see Fig. 2A). This yielded A_0 for the first and A_∞ for the last EPSC in a train. We define A_∞ as the *steady-state* AMPA EPSC, and A_∞/A_0 as the relative steady-state amplitude. Both at –70 mV and –40 mV, a slow drift in the baseline during subsequent EPSCs in a train generated a *sustained current* (A_s). At –70 mV A_s was interpreted according to the Di Gregorio et al. (2002) hypothesis and our recent work (Sola et al., 2004) demonstrating a persistent activation

of AMPA receptors by glutamate spillover. At –40 mV, A_s was largely dependent on NMDA receptor activation. The NMDA current was obtained by subtraction of the AMPA current from composite EPSCs at –40 mV, where Mg^{2+} block on NMDA channels is largely removed (Rossi et al., 2002). The AMPA current was determined at –70 mV and peak-scaled to the 1st EPSC at –40 mV (see Fig. 3A). The underestimate due to residual NMDA currents at –70 mV (probably caused by NR2C subunits) is negligible (≤10%). The NMDA current was measured 8 ms after each stimulus, where NMDA EPSC amplitude is close to peaks (Fig. 3A; see also Rossi et al., 2002). Recordings in which the extracellular Ca^{2+} concentration was changed were performed in the presence of the NMDA receptor blockers APV and 7Cl-Kyn.

The cerebellar granule cell has a compact structure and behaves like a lumped electrotonic compartment (D'Angelo et al., 1995; Silver et al., 1996b). Analysis of passive current transients induced by 10-mV hyperpolarizing voltage steps from the holding potential of -70 mV (low-pass filter = 10 kHz, sampling rate = 100 kHz) yielded input capacitance C_m= 4.1±0.2 pF, membrane input resistance R_m=2.7±0.4 GΩ, and series resistance R_s=21.2±1.5 MΩ. These parameters did not show significant variation at the end of recordings (C_m= 3.3±0.3 pF, R_m=3.3±0.4 GΩ, R_s=27.2±4.4 MΩ) demonstrating recording stability.

Mathematical modeling of repetitive synaptic transmission

We have developed a mathematical model in order to interpret repetitive neurotransmission and its effects on neuronal excitation at the cerebellum mossy fiber – granule cell synapse. Our aim was to conjugate fundamental aspects of neurotransmission derived from past and present recordings with a detailed reconstruction of postsynaptic electroresponsiveness. The model was developed with the NEURON simulator (Hines and Carnevale, 2001). To make model temperature (T_{mod}) compatible with experiments, rate constants in receptor kinetic schemes and voltage-dependent currents were corrected for the actual experimental temperature (T_{exp}=30 °C) using a Q_{10}=3 according to the relation $Q_{10}^{(Tsim-Texp)/10}$ (D'Angelo et al., 2001).

The granule cell model was derived from our previous paper (D'Angelo et al., 2001) and updated based on recent experimental measurements. I_{K-A} was weakened (activation rates were reduced by 6 times, inactivation rates were reduced by 3 times, steady-state activation was shifted by 8.7 mV in the depolarizing direction with voltage-dependence 0.059 mV^{-1}, and g_{max} was reduced to 0.0032 S/cm^2; Maffei, Rossi and D'Angelo, unpublished observation), I_{Na-r} and I_{Na-p} density were updated ($2 \cdot 10^{-4}$ S/cm^2 and $2 \cdot 10^{-5}$ S/cm^2; Magistretti, Castelli and D'Angelo, unpublished observation), I_{K-IR} density was set at $2.655 \cdot 10^{-4}$ S/cm^2 (Rossi, Roggeri, Gall, de Kerchove d'Exaerde, Schiffmann, Taglietti, D'Angelo, unpublished observation), and the contribution of

GABA-leakage was increased ($3 \cdot 10^{-5}$ mS/cm^2; Rossi et al., 2002). Since the granule cell is electrotonically compact (Silver et al., 1996b; D'Angelo et al., 1995; Cathala et al., 2003), there was no need to simulate dendrites and the original mono-compartmental structure was maintained. Cerebellar granule cells receive 4 mossy fiber inputs on average (Eccles et al., 1967), each one impinging on a dendrite placed in a different glomerulus. The glomerulus is formed by a large mossy fiber terminal facing about 50 granule cell dendrites in the rat (Jakab and Hamory, 1988). Since glomeruli are physically isolated (they are enveloped into a glial sheet and are spaced by more than 10 micrometers) and since EPSCs scale almost linearly during synaptic recruitment (Di Gregorio et al., 2003; Sola et al., 2004), the model was implemented with 4 identical independent synapses.

Simulation of a single EPSC basically needs that a neurotransmitter waveform activates a receptor kinetic scheme (Destexhe et al., 1994). Simulation of an EPSC train is more problematic not only because presynaptic dynamics must be computed but also because postsynaptic receptor states evolve in time maintaining the history of previous events. The situation is complicated at a multi-site synapse by the stochastic activation of different receptor clusters and by neurotransmitter diffusion between sites (Barbour, 2001). In principle, if the synaptic structure and diffusion coefficient are known, Monte-Carlo simulations with several releasing sites would solve the problem allowing each receptor to develop its individual time-dependent history. However the stochastic nature of the output would require repetition over a large number of simulations to obtain average responses making the method impractical for EPSC train fitting. We have therefore adopted the approximation of making neurotransmitter concentration T proportional to a presynaptic variable Y reporting the intensity of neurotransmitter release (Buonomano, 2000).

Presynaptic dynamics. Mossy fiber – granule cell EPSCs show facilitation and depression (Xu-Friedman and Regehr, 2003; Sola et al., 2004; this paper), so that presynaptic dynamics need to be explicitly modeled. The presynaptic model has been derived from the Tsodyks and Markram (1997) 3-state scheme (Tsodyks et al., 2000) in which X represents transmitter resources available for release (possibly synaptic vesicles), Y released transmitter, and Z recovered transmitter. Transition between states is governed by first order reactions according to a 1st order differential equation system

$$(1)\begin{cases}\dfrac{dX}{dt}=\dfrac{Z}{\tau_R}-P\cdot X\cdot\delta\left(t-t_{spike}\right)\\ \dfrac{dY}{dt}=-\dfrac{Y}{\tau_I}+P\cdot X\cdot\delta\left(t-t_{spike}\right)\\ \dfrac{dZ}{dt}=\dfrac{Y}{\tau_I}-\dfrac{Z}{\tau_R}\\ \dfrac{dP}{dt}=-\dfrac{P}{\tau_F}+p\left(1-P\right)\cdot\delta\left(t-t_{spike}\right)\end{cases}$$

in which τ_R is the time constant of recovery of releasable transmitter, τ_F is the time constant of facilitation, τ_I the time constant of inactivation, P is release probability and p its initial value, and δ is Dirac's delta function. While $X(t)$, $Y(t)$ and $P(t)$ are discontinuous functions, the system is solved analytically by integrating differential equations in intervals $[t_{spike,n}, t_{spike,n+1}]$ for initial conditions at time $t_{spike,n}$. At times $t=t_{spike}$ the values of functions are changed abruptly by $p \cdot X$ or $P(1-p)$. This causes that, when a spike arrives, a proportion P of the resource X is transferred to Y. Depletion of the resource X causes synaptic depression (another component depends on postsynaptic receptor desensitization, see below). Synaptic facilitation is governed by p activity-dependence.

Postsynaptic receptor activation. Granule cell postsynaptic responses are generated both through direct release from active zones onto corresponding postsynaptic receptors and through spillover of glutamate from neighboring releasing sites (DiGregorio et al., 2002; Cathala et al., 2003). For AMPA receptors, which are located into the cleft, glutamate concentration was obtained combining a synaptic pulse (T_s) with a diffusion wave (T_d). Synaptically released glutamate acting on AMPA receptors was generated with a 1 mM - 0.3 ms squared pulse, which was shown to well approximate transmitter action in the cleft (Destexhe et al., 1994). The effective glutamate concentration in the cleft is therefore

$$(2)\qquad T= T_s + T_d = Y\cdot [T_{s(max)} + T_{d(max)}]$$

where $T_{s(max)}$ and $T_{d(max)}$ are maximum concentrations. NMDA receptors, which are largely extrasynaptic (Rossi et al., 2002; Cathala et al., 2003) were activated by glutamate diffusion, T_d.

Glutamate binding to postsynaptic receptors activates kinetic schemes governed by microscopic first-order transitions (see Fig. 6-7), leading to the open state, $O(T)$. It follows that

$$(3)\qquad i= g\cdot\Delta V = g_{max}\cdot O(T)\cdot (V-V_{rev})$$

where V_{rev} is the ionic reversal potential and g_{max} the maximum synaptic conductance for either NMDA or AMPA channels.

AMPA receptor kinetic scheme. Several investigations have assessed the properties of AMPA receptor-mediated currents in cerebellar granule cells. The time course of AMPA EPSCs in granule cells and estimates for AMPA channel open probability were reported *in situ* (DiGregorio et al., 2002; Sola et al., 2004). AMPA receptor desensitization was investigated in granule cell patches in culture (Silver et al., 1996a). This allowed to reconstruct a simple DCO AMPA receptor kinetic scheme (Fig. 6A) using a parameterization similar to that recently reported by Saftenku (2005), with ko_+=5.4 ms^{-1}, ko_-=0.82 ms^{-1}, kd_+=1.12 ms^{-1}, kd_-=0.013 ms^{-1}, K_B=0.44 mM, $S=T^2/(T+K_B)^2$. By using the PSD conductance (180-267 pS) and receptor open probability (0.4-0.6) measured with non-stationary fluctuation analysis (Traynelis et al., 1993; Silver et al., 1996b), the maximum conductance at a single mossy fiber – granule cell synapse with 2-4 releasing sites lay between 900-1780 pS. Indeed, with 1200 pS and p=0.4 (Sola et al., 2004) the model correctly simulated unitary EPSC amplitude.

NMDA receptor kinetic scheme. There are no specific kinetic schemes for NMDA receptor-mediated currents in cerebellar granule cells. Since most of the NMDA current is determined by NMDA receptors with low open probability (Rossi et al., 2002), we adopted the corresponding kinetic scheme developed by Rosenmund et al. (1995) for cortical neuronal cultures. There are two identical closed states and the desensitized state is entered from the second closed state, with k_{1+}=5 $mM^{-1}ms^{-1}$, k_{1-}=0.1 ms^{-1}, k_{2+}=5 $mM^{-1}ms^{-1}$, k_{2-}=0.1 ms^{-1}, ko_+=0.03 ms^{-1}, ko_-=0.966 ms^{-1}, kd_+=0.00012 ms^{-1}, kd_-=0.009 ms^{-1} (see Fig. 6B). Glutamate binding/unbinding reactions were slightly slowed down to better follow NMDA EPSC rising kinetics and receptor desensitization was reduced to prevent early decay of NMDA receptor-dependent depolarization during repetitive synaptic activity (D'Angelo et al., 1995). These adaptations were justified by considering the incomplete knowledge of NMDA receptor regulation in granule cells. Since Mg^{2+} block is very fast compared to other transitions, it is regarded as instantaneous. Thus, $g_{NMDA}=g_{NMDA(max)} \cdot O \cdot B$, where

$$B = \frac{1}{1+\exp^{-\left(\frac{V-V_0}{k}\right)}} \tag{4}$$

represents Mg^{2+} block. This Boltzmann equation, was fitted to the data in Rossi et al. (2002) obtaining k=13 mV (steepness of voltage dependence) and V_0=-20 mV (half-activation potential).

By using 376 low open-probability channels with a single channel conductance of 50 pS, as indicated by MK801 blocking kinetics (Rossi et al., 2002), the maximum NMDA EPSC conductance is 18800 pS per synapse. With this value, activation of the NMDA receptor model (Rosenmund et al., 1995) by glutamate spillover (Cathala et al., 2003) reproduced experimental NMDA receptor-mediated EPSCs.

EPSC fitting and glutamate diffusion. Since the diffusion space is unknown in principle, its properties were inferred by fitting the model to AMPA EPSCs, which were shown to include a sizeable spillover-mediated component (Di Gregorio et al., 2002). Fits were performed using a SIMPLEX routine implemented in NEURON (see Fig. 6C). We preliminary performed AMPA EPSC fits using a diffusion kernel with free geometry (Neher and Sakaba, 2001). Iterative adjustment of diffusion parameters fitted the whole EPSC, including both the direct and indirect component, with 2D geometry. Thus, inter-site glutamate diffusion (Barbour, 2001) was represented as

$$T_{d(\max)}(r,t) = \frac{M}{h \cdot 4\pi D_{eff} t} \exp\left(-\frac{r^2}{4 D_{eff} t}\right) \qquad (5)$$

in which M is the number of released molecules, D_{eff} is the effective diffusion coefficient, r is the distance from glutamate source, and h is cleft height (Crank, 1975). While h was fixed at 20 nm, D_{eff}, r, and M were obtained by fitting the first EPSC in a train. Then, D_{eff}, r, and M were fixed and we obtained τ_R, τ_F and p by fitting the whole EPSC train. An example of this procedure is reported in figures 5A2 and 6 and the corresponding average data are reported in Table 1.

It should be noted that using 2D geometry might lead to overestimate spillover glutamate concentration and its effect on desensitization (Xu-Friedman and Regehr, 2003), thereby reducing the relative importance of presynaptic vesicle recovery during short-term depression. Although a definite conclusion on the balance between desensitization and vesicle depletion in determining synaptic depression cannot be drawn at the present stage, we note that values obtained by fitting were consistent with current knowledge on mossy fiber – granule cell transmission (see Table 1), so that using a 3-state AMPA scheme and 2D diffusion provided a minimal effective model of repetitive synaptic transmission in the cerebellar glomerulus. A comparison was done using more complex AMPA receptor kinetic schemes. While the Diamond and Jahr (1997) scheme was also effective, the Wadiche and Jahr (2001) and Raman and Trussell (1995) schemes desensitized too fast and failed to reproduce the spillover mediated component in EPSC trains (data not shown).

RESULTS

In this paper we have investigated the impact of LTP on granule cell neurotransmission during repetitive mossy fiber activity.

LTP regulates granule cell burst initiation and frequency

The effect of short stimulus trains on mossy fiber – granule cell responses was initially investigated by D'Angelo et al., (1995), who revealed AMPA receptor-mediated EPSP depression and an important contribution of sustained NMDA receptor-mediated responses to EPSPs temporal summation. Here, EPSPs were recorded using minimal stimulation from the initial membrane potential of –71.5±0.5 mV. EPSPs measured 17.8±2.7 mV, peaked in 8.2±1.5 ms, and showed a duration at half-amplitude (HW) of 24.5±4.3 ms (n=10). During a train of 10 impulses at 100 Hz, individual EPSPs showed a marked depression but their temporal summation caused a progressive depolarization followed by spike discharge (Fig1A).

LTP was induced by theta-burst stimulation (see Armano et al., 2000) leading to a 39.2±5.3% EPSP amplitude increase 15 min after induction. At the same time, EPSP temporal summation in response to mossy fiber spike trains was enhanced. The first-spike delay significantly decreased from 41.7±10.4 ms to 17.3±11.2 ms (n=7; $p<0.01$) and the average firing frequency increased from 20.7±6.7 Hz to 49.9±10.8 Hz (n=7; $p<0.01$). The potential coexistence of persistent changes in intrinsic excitability (Armano et al., 2000) was evaluated by measuring the first-spike delay and spike frequency during injection of depolarizing current pulses (Fig. 1B). These recordings showed that LTP was indeed associated with earlier initiation (16.3±6.2 ms; n=7) and increased frequency (17.4±4.3 Hz; n=7) of spikes independent from synaptic inputs. The changes in delay observed using depolarizing current pulses were significantly smaller than those observed using repetitive mossy fiber stimulation ($p<0.01$; n=7), while the difference in firing frequency was not statistically significant (Fig. 1C).

***** Fig. 1 *****

This observation suggests a sizeable contribution of synaptic changes to first-spike delay regulation. In order to determine the underlying synaptic mechanisms, we have measured the response to EPSC trains in voltage-clamp and reconstructed the voltage response with a mathematical model. Here below we report the analysis of EPSC train dynamics for the AMPA and NMDA currents, which have different receptor gating and kinetics and could give substantially different contribution to synaptic excitation.

Short-term plasticity during LTP: the AMPA EPSCs

AMPA currents were isolated at –70 mV (Fig. 2A), where the driving force is favorable and NMDA channels are largely blocked by Mg^{2+} (cf. Fig. 3A below). EPSC trains at 100 Hz showed *rapid AMPA receptor-mediated transitions* sitting over a *sustained current* most probably corresponding to slow summation of glutamate spillover currents (these parameters are further defined in the Methods and illustrated in Fig. 2A). AMPA spillover currents can be observed in single EPSCs and are thought to arise from glutamate released from neighboring sites in the glomerulus (DiGregorio et al., 2002; Sola et al., 2004). We recall that glutamate spillover at mossy fiber synapses is particularly intense owing to the special architecture of the cerebellar glomerulus, which is constituted of about 50 closely spaced synaptic connections enwrapped into a glial sheet (Eccles et al., 1967; Xu-Friedman and Regehr, 2003).

The transient component of AMPA EPSCs showed depression in 75% of cases (n=12) (Fig. 2B), while an initial transient facilitation followed by depression was observed in the remaining 25% (n=4) of cases. In only-depressing trains, the amplitude of AMPA EPSCs decreased nearly exponentially allowing to estimate the depression time-constant, τ_d=15.4±2.2 ms (n=8), and the relative steady-state EPSC amplitude, A_∞/A_0=0.25±0.03 (n=8) (Fig. 2C). The sustained current increased attaining a steady-state after 2-3 impulses.

LTP was induced by TBS paired with membrane depolarization at –40 mV to allow Ca^{2+} influx through NMDA channels (D'Angelo et al., 1999). During LTP, the first AMPA EPSC increased by 43.1±13.9% (n=16). In the 8 depressing synapses, EPSC depression became faster with τ_d=10.4±2.2 ms (n=8; $p<0.01$, paired *t*-test). Moreover, the steady-state A_∞ remained almost unchanged causing a significant decrease in the relative steady-state, A_∞/A_0=0.16±0.02 (n=8; $p<0.01$, paired *t*-test). In the 4 facilitating synapses, facilitation turned into depression. In all cases the sustained current showed a significant increase of 22.1±9.7% (n=16; $p<0.05$) at the end of the train. In agreement with the observation reported by Sola et al., (2004), the switch from facilitation to depression and the A_∞/A_0 and τ_d changes during LTP are characteristic of an increased presynaptic vesicle turnover (Tsodyks and Markram, 1997; O'Donovan and Rinzel, 1997; Brenowitz and Trussell, 2001), although the changes could also be influenced by postsynaptic receptor desensitization (Xu-Friedman and Regehr, 2003).

***** Fig. 2*****

Short-term plasticity during LTP: the NMDA EPSCs

The NMDA current was isolated at –40 mV, where NMDA channels are unblocked from Mg^{2+} (Fig. 3A). This choice was further motivated by the observation that the NMDA current in granule cells has voltage-dependent kinetics (NMDA-EPSCs slowdown with depolarization; D'Angelo et al., 1994) and that the membrane potential of –40 mV is critical for NMDA receptor regulation of EPSP temporal summation and spike firing, providing the data used for mathematical modeling (see below).

Fig. 3A shows that the sustained component in 100 Hz EPSC trains was similar at –40 mV and at –70 mV despite the reduction in driving force for AMPA currents, revealing the voltage-dependent contribution of the NMDA current. Subsequent application of 10 μM CNQX, a specific blocker of non-NMDA ionotropic receptors, yielded the NMDA component in isolation. At –40 mV the NMDA current accounted for most of the sustained current (Fig. 3A, middle right traces ; 2.2±0.1 pA at the end of trains, n=4), showed a marked temporal summation and a smooth time-course. At –70 mV the NMDA current was negligible (0.5±0.1 pA, n=4). Accordingly, the current obtained by subtracting the scaled trace at –70 mV from that at –40 mV corresponded precisely to the NMDA current isolated pharmacologically (2.2±0.2 pA at the end of trains, n=4; $p<10^{-6}$). Subsequent addition of 100 μM APV and 50 μM 7Cl-Kyn completely blocked the responses, ruling out any sizeable contribution of re-uptake currents.

By applying the subtraction procedure (see also Methods), we could determine the time course of the NMDA current in the same recordings used to construct Fig. 2 without needing of pharmacological tools. During LTP (Fig. 3B), the 1st NMDA EPSC increased by 53.3±16.0% (n=4; $p<0.0007$), while the steady-state response did not significantly change (5.2±6.1%, n=4; NS). Thus, potentiation in NMDA differed from that in AMPA current trains, although both showed LTP on the 1st EPSC. As discussed below, the apparent saturation of responses during trains could reflect saturation of NMDA receptors due to glutamate accumulation.

***** Fig. 3*****

*Neurotransmission dynamics are regulated by release probability*In order to understand whether increasing release probability could determine the changes in EPSC trains observed during LTP, release probability was modified with different extracellular Ca^{2+}/Mg^{2+} ratios (Fig. 4; Katz and Miledi, 1968; Dodge and Rahamimoff, 1967). In these recordings we used 50 Hz EPSC trains and NMDA receptors were blocked with 100 μM APV and 50 μM 7Cl-Kyn in order to prevent any NMDA receptor-dependent form of synaptic plasticity. At *low* Ca^{2+}/Mg^{2+} ratio (0.5 mM Ca^{2+}, 2.8

mM Mg^{2+}) all granule cells showed a prominent EPSC facilitation. At *normal* Ca^{2+}/Mg^{2+} ratio (2 mM Ca^{2+}, 1.2 mM Mg^{2+}) 8 out of 11 granule cells showed depression, the remaining showed facilitation. At *high* Ca^{2+}/Mg^{2+} ratio (4 mM Ca^{2+}, 0 mM Mg^{2+}) all recordings showed depression. Thus, when facilitation was not observed at normal Ca^{2+}/Mg^{2+} ratio, this was due to a high initial release probability causing prominent depression. It should also be noted that increasing Ca^{2+}/Mg^{2+} ratio from normal to high caused changes that closely mimicked those observed during LTP. A_0 showed a significant 39.9±7.8% increase (n=8; $p<0.01$), A_∞/A_0 showed a reduction from 0.22±0.04 to 0.13±0.03 (n=8; $p<0.01$), and a marked increase in the sustained current (28.2±7.5%; n=8; $p<0.01$). These changes were not statistically different from those obtained during LTP (Fig. 4C). Thus, the changes induced in AMPA EPSC trains by raising release probability mimicked those observed during LTP supporting their presynaptic origin.

***** Fig. 4 *****

Modeling EPSC trains and their changes during LTP

In order to verify whether the EPSC train changes observed during LTP could explain those in current-clamp recordings, we developed a mathematical model (see Methods) incorporating the three main factors regulating mossy fiber – granule cell neurotransmission, namely (i) presynaptic release dynamics, (ii) neurotransmitter spillover, and (iii) microscopic kinetics of postsynaptic receptors. The model was useful to circumvent a series of experimental obstacles. Most notably, modifications in neurotransmitter release probability obtained by manipulating calcium concentration profoundly alter postsynaptic electroresponsiveness and the coexistence of non-synaptic plasticity prevents a precise analysis of the contribution of synaptic changes.

In the model, AMPA EPSCs were composed of a fast direct and a slow indirect spillover-mediated component (Fig. $5A_1$; Di Gregorio et al., 2002). NMDA EPSCs were activated by glutamate spillover, were small and slow compared to AMPA EPSCs, were largely blocked at resting membrane potential and unblocked in the threshold region (Fig. $5B_1$; Rossi et al., 2002; Cathala et al., 2003). The model fitted both the AMPA (Fig. $5A_2$) and the NMDA current (Fig. $5B_2$) during regular 100 Hz trains. Given the stochastic nature of mossy fiber discharge in response to single tactile stimuli (Chadderton et al., 2004), we also tested the ability of the model to fit random spike trains. To this aim, the stimuli were generated according to a Poisson distribution with an average frequency of 50 Hz. Despite in these trains the inter-stimulus intervals varied from a few to tens of milliseconds, the model could still fit the EPSCs (Fig. 6). Average parameters obtained from fittings were not statistically different when using either regular or random trains (Table 1).

The value of p was close to that estimated using quantal analysis in this same synapse (Sola et al., 2004). Diffusion parameters are in agreement with the analysis reported by Saftenku (2005). The parameter M indicates the number of molecules diffusing from a distance r. With M=21500 and p=0.42, assuming ~4000 glutamate molecules per synaptic vesicle (SV; Barbour, 2001) and 1 SV/site (Sola et al., 2004), there would be M/(4000*p)=12.8 releasing sites contributing to spillover. The corresponding density over a circular surface with r=1 μm is 3.9 sites/μm^2, in the range of values measured with electron-microscopy (average of 2.9 sites/μm^2, Xu-Friedmann and Regehr, 2003). It should also be noted that r lays between the inter-site distance and the glomerular radius, and that the number of releasing sites is within the limits expected for the glomerulus (Xu-Friedmann and Regehr, 2003; see also Saftenku, 2005, for review of literature data). D_{eff} is very close to the value recently estimated in the cerebellar glomerulus (0.33 μm^{2}ms^{-1} at 37 ^{o}C; Nielsen et al., 2004). There are no previous experimental estimates for τ_F and τ_R in this synapses, but the values fall in the range reported for other central synapses (Tsodyks and Markram, 1997; Gupta et al., 2000).

Thus, the model can predict repetitive neurotransmission in the cerebellar glomerulus with physiologically meaningful parameters. Unless differently stated, the values reported in Table 1 for regular stimulus trains will be used for further simulations in the paper.

**** Figs 5 and 6 ****

A validation of the model comes from its ability to account for known properties of postsynaptic channel activation (Fig. 7). During trains, spillover increases the sustained AMPA current and at the same time accelerates AMPA receptor desensitization, so that EPSC depression during trains depends both on pre- and postsynaptic factors, as predicted by Xu-Friedman and Regehr (2003). Raising the initial p from 0.4 to 0.6, which approximates the changes observed during LTP (Sola et al., 2004), accelerated glutamate depletion and increased glutamate spillover. These changes predicted a series of experimental effects (cf. Figs. 1-4): (i) AMPA EPSC synaptic depression accelerated with a marked decrease in the A_∞/A_0 ratio (facilitation emerged at p<0.3, not shown); (ii) the sustained AMPA current increased without saturating (Silver et al., 1996b); (iii) the NMDA current increased in the first few pulses but then saturated. Quantitatively, the p increase caused a 35% potentiation in the first EPSC, a 19% increase in the sustained current, and a 38% decrease in A_∞/A_0, close to experimental observations. Thus, the model accounted for the main aspects of glomerular physiology and predicted the changes in EPSC trains occurring during LTP.

**** Fig. 7 ****

Modeling synaptic excitation and its changes during LTP

The model could reproduce granule cell EPSPs and their effect on synaptic excitation. Indeed, coupling AMPA and NMDA synaptic conductances with a detailed reconstruction of granule cell intrinsic excitability (D'Angelo et al., 2001) reproduced the main aspects of granule cell synaptic excitation (Fig. 8A, B) As reported by D'Angelo et al. (1995), (i) EPSPs generated by synchronous activation of 2 mossy fibers were slower than single fiber EPSPs due to NMDA current unblock during depolarization; (ii) synchronous activation of 3 mossy fibers was needed to generate an action potential from rest (-70 mV in the model), and a doublet of action potentials was generated with 4 mossy fibers; (iii) repetitive stimulation generated repetitive spike discharge. Interestingly, despite their small size, NMDA and AMPA spillover currents generated a considerable depolarization enhancing EPSP temporal summation, EPSP-spike coupling, and firing (Fig. 8B). This effect was due to the high input resistance of granule cells (in the GΩ range, see Methods), so that even a few pA sustained current generated a remarkable depolarizing action.

The model allowed to dissect the effect of presynaptic changes on firing from those due to intrinsic electroresponsiveness. Fig. 8C demonstrates the ability of the model to reproduce the main effect of LTP on spike trains: by raising p, the first spike delay decreased and spike frequency was maintained.

**** Fig. 8 ****

Theoretical predictions on the LTP mechanism

The involvement of spillover in LTP expression was tested by restricting the p change to the direct component (p_{dir}), while p of the indirect component (p_{ind}) was fixed. Clearly, this simulation makes the case of potentiation occurring only in the releasing sites facing the granule cell dendrite under investigation. With p_{ind}=0.4, changing p_{dir} did not cause any noticeable modulation in spike delay and frequency (Fig. 9A, C). Thus, probably, the whole glomerulus was potentiated in our experiments.

The classical alternative to a p raise is an increase in maximum postsynaptic conductance, g_{max}. By raising p (Fig. 9B, C), repetitive activation of one synapse yielded large spike delays and relatively low firing frequencies, as observed in recordings performed with minimal stimulation. Conversely, a proportional change in g_{max} (for both AMPA and NMDA receptors) with p fixed at 0.4 caused poor modulation of spike delay and steep modulation of firing frequency. The difference

highlights the effectiveness of presynaptic regulation of neurotransmission dynamics, which allows slow progressive EPSP temporal summation at low *p* causing long delays. Thus, changing *p* or g_{max} is not equivalent in terms of synaptic dynamics, although the effect on an isolated EPSP would be indistinguishable.

**** Fig. 9 ****

Theoretical predictions on the role of non-synaptic changes

Simulations shown in Figures 8C and 9C suggest that earlier burst initiation during LTP is largely due to enhanced neurotransmitter release, and therefore to a presynaptic mechanism. Conversely, the increased firing frequency could be mostly explained by changes in intrinsic excitability, and be postsynaptic in nature.

In a series of simulations we modified intrinsic excitability by changing ionic current density or gating (Fig. 10A). Although we tested just some of the possible mechanisms of regulation (see for review Debanne et al., 2003), these examples have been grounded on the hypothesis proposed by Armano et al. (2000) and help understanding how the changes observed during LTP might originate (see Fig. 10 for details). We have therefore modified the density of the M-current ($I_{K\text{-}M}$), the density of the persistent Na^+ current ($I_{Na\text{-}p}$), and the threshold of the transient Na^+ current ($I_{Na\text{-}t}$). The firing frequency increase was obtained, in order of efficacy, by: ($I_{K\text{-}M}$ x 0.12) > ($I_{Na\text{-}p}$ x 1.5) ≈ ($I_{Na\text{-}t}$ activation –3mV). The first-spike delay reduction was obtained, in order of efficacy, by: ($I_{Na\text{-}p}$ x 1.5) ≈ ($I_{Na\text{-}t}$ activation –3mV) > ($I_{K\text{-}M}$ x 0.12). Combinations of these changes proved particularly effective in reproducing the experimental results (Fig. 10B). Among other possible changes, reducing the Ca^{2+}-dependent current ($I_{K\text{-}Ca}$) was ruled out since it caused repetitive bursting (D'Angelo et al., 2001), a firing pattern not observed during LTP (data not shown).

When the changes in $I_{K\text{-}M}$, $I_{Na\text{-}p}$ and $I_{Na\text{-}t}$ were associated with a *p* increase from 0.4 to 0.6, we observed a good matching with experimental measurements obtained during repetitive synaptic transmission (cf. Fig. 1C). Simulations showed that the contribution of pre- and post-synaptic changes was not simply additive. The presynaptic change dominated delay regulation and was modestly improved by changes in intrinsic excitability. Conversely, postsynaptic changes dominated frequency regulation, which was poorly improved by changes in release. These simulations suggest therefore that delay and frequency are to a considerable extent subjected to differential regulation by pre- and postsynaptic mechanisms of potentiation.

**** Fig. 10 ****

DISCUSSION

The main result in this paper is that increased release probability during LTP, by regulating short-term facilitation and depression, caused earlier activation of cerebellar granule cell spike bursts elicited by repetitive mossy fiber activity. The presynaptic mechanism coexisted with postsynaptic regulation of ionic channels, which played a major role in determining the granule cell output firing frequency.

Repetitive neurotransmission at the mossy fiber – granule cell relay of cerebellum

Repetitive synaptic activity at the cerebellar mossy fiber – granule cell relay determined complex temporal dynamics in EPSC trains. In response to a 100 Hz burst, the most prominent behavior was short-term depression leading AMPA EPSCs toward a reduced steady-state in about 5 pulses. A transient short-term facilitation affecting the first 2-3 EPSCs emerged at low release probability. In addition, AMPA and NMDA receptor activation generated a sustained current, which showed marked temporal summation during trains. The sustained current was probably the extension of the spillover currents recorded in single EPSCs (Cathala et al., 2003; DiGregorio et al., 2002; Xu-Friedman and Regehr, 2003). These processes provided the key to interpret EPSP trains and spike firing (this paper, see also D'Angelo et al., 1995) and their changes during LTP.

Two aspects indicated that, as reported by Sola et al. (2004), the expression of LTP depended on increased release probability. First, either raising extracellular [Ca^{2+}] or eliciting LTP enhanced AMPA EPSC depression leading to a common steady-state (A_∞) (cf . Tsodyks and Markram, 1997). Secondly, raising extracellular [Ca^{2+}] or eliciting LTP enhanced the sustained AMPA and NMDA receptor-mediated currents. It should be noted that sustained AMPA and NMDA currents did not show an identical behavior. The sustained AMPA current was potentiated over the entire train, suggesting that AMPA receptors are not saturated, as observed at this (Silver et al., 1996b; DiGregorio et al., 2002) and other central synapses (McAllister and Stevens, 2000). The sustained NMDA current showed LTP in the first (e.g. D'Angelo et al., 1999) but not in later responses. Thus, probably, NMDA receptors are not saturated by a single pulse (McAllister and Stevens, 2000; Mainen et al., 1999) but tend to saturate during repetitive stimulation.

Modeling repetitive neurotransmission

Mathematical modeling helped visualizing the interplay of the 3 main processes supposed to govern neurotransmission dynamics, namely (i) turnover of presynaptic resources (vesicle cycling), (ii) glutamate diffusion, and (iii) postsynaptic receptor gating.

During trains, presynaptic resource depletion and postsynaptic receptor desensitization caused AMPA EPSC depression, as predicted by Xu-Friedman and Regehr (2003). AMPA, unlike NMDA receptors, did not tend to saturate during trains. Spillover in the model generated sustained AMPA (DiGregorio et al., 2002) and NMDA currents (Cathala et al. 2003). There was no need in the present simulations to account for a second NMDA receptor population, which proved to have a distinct sensitivity to spillover (Rossi et al., 2002). With input bursts longer than those used in the present simulations (>150 ms), the NMDA current may be reduced by slowly-developing processes like glutamate re-uptake (Overstreet et al., 1999).

By raising *p*, four main experimental observations were predicted (this paper and Sola et al., 2004; see also DiGregorio et al., 2002; Xu-Friedmann and Regehr, 2003): (1) the 1st EPSC increased, (2) AMPA EPSC depression accelerated, (3) a common steady-state was attained, and (4) glutamate spillover increased enhancing the sustained AMPA and NMDA currents. It should be noted that spillover promoted both AMPA receptor activation and desensitization (Fig. 7), preventing *de facto* a net change with release probability of AMPA EPSCs at steady-state. Thus, the model behaved as expected from a pure presynaptic mechanism, in which the steady-state EPSC amplitude does not change with release probability (Tsodyks and Markram, 1997; O'Donnovan and Rinzel, 1997; Brenowitz and Trussell, 2001).

Pre- and postsynaptic mechanisms determining mossy fiber – granule cell LTP

Mossy fiber – granule cell LTP is a composite process involving a pre-synaptic increase of release probability (Sola et al., 2004) and a postsynaptic increase in intrinsic excitability (Armano et al., 2000). The observation that, during LTP, shortening of first spike delay was significantly more pronounced with repetitive synaptic activation than with depolarizing current injection, indicates that the pre- and postsynaptic components preferentially control different aspects of granule cell excitation. The analysis of EPSC trains and mathematical modeling revealed the underlying mechanism: EPSP temporal summation is critical for reaching spike threshold but, once firing begins, it is efficiently regulated by postsynaptic ionic conductances. Due to the complexity of the system, it seems worth summarizing current understanding about the main mechanisms contributing to potentiate the response of granule cells during LTP.

a) Increasing release probability determines an initial EPSC potentiation followed by a protracted spillover current. The AMPA and NMDA currents play distinct roles in this mechanism. The increase of the AMPA current, through its large transient component, would particularly important to promote coincidence detection of activity in more than one mossy fiber (Chatala et al., 2004). A substantial contribution to EPSP temporal

summation, which was revealed by activating single mossy fibers from rest, was determined by spillover-mediated activation of sustained AMPA and NMDA currents. Increased spillover during LTP contributed not just to maintain repetitive spike discharge counteracting synaptic depression, but also to accelerate membrane depolarization and spike activation.

b) Increasing granule cell intrinsic excitability regulates both granule cell firing initiation and frequency (D'Angelo et al., 2001). During LTP, control on firing frequency is greater than control on delay. This effect could be reproduced by reducing $I_{Na\text{-}t}$ threshold, raising $I_{Na\text{-}p}$ and reducing $I_{K\text{-}M}$ density, consistent with the hypothesis proposed by Armano et al. (2000) predicting a raise in Na^+ and a decrease in K^+ currents activating in the just sub-threshold region.

The effect of release probability on glomerular information processing

A relevant prediction of the model is that changing *p* favors modulation of burst delay (at least at $p<0.3$) whereas changing postsynaptic conductance favors modulation of firing frequency. Moreover, the model predicts that potentiation should occur at multiple sites in the mossy fiber terminal in order to raise spillover and obtain a reliable delay and frequency modulation. This effect is not surprising, since TBS also activates other granule cells impinging on the glomerulus (about 50 per mossy terminal in the rat; Jakab and Hámori, 1988). It is therefore possible that LTP in these recordings reflects a collective potentiation, as discussed in Maffei et al. (2003). These results suggest that synapses differing for pre- or postsynaptic LTP expression or for the intensity of spillover (Bliss et al, 2003; Lisman, 2003) could differ in their ability to process spike sequences in the time and frequency domain (Rieke et al., 1996; Tsodyks and Markram, 1997). For instance, at hippocampal synapses evidence for postsynaptic expression is compelling (for review see Malenka and Nicoll, 1999) and spillover enhances the NMDA but not the AMPA response (Kullman et al., 1996), while at central auditory synapses increasing release enhances EPSC depression without apparent involvement of spillover currents (Brenowitz and Trussell, 2001). At hippocampal synapses, LTP preserves the fidelity of postsynaptic responses to presynaptic bursts (Selig et al., 1999), suggesting that there are differences in the way neuronal circuits use modifications in synaptic strength to encode new information.

These results extends the implications for burst processing at central synapses. Bursts have been proposed (i) to provide a safety mechanism against synaptic unreliability, (ii) to generate short-term temporal dynamics, and (iii) to re-code the temporal structure of input spike trains (Lisman, 1997; Krahe and Gabbiani, 2004). Here we show that burst processing provides an

adaptable control over output spike initiation depending on release probability. Although we have limited our analysis to *p* regulation by LTP, bidirectional plasticity may be a natural extension of the present observations toward LTD (Gall et al., 2005).

Regulation of granule cell burst initiation could implement adaptable delay lines affecting downstream activation of the cerebellar circuitry. Precise timing of granule cell spikes is critical to determine parallel fiber – Purkinje cell coincidence detection and hence LTD and LTP (Han et al., 2000; Coesmans et al., 2004). Maintenance of a sustained bursting is also critical for inducing parallel fiber – Purkinje cell LTD and LTP (Wang et al., 2000; Casado et al., 2002). Moreover, bursts, by causing facilitation and temporal summation, determine reliable activation of synapses between parallel fibers and their targets, including Purkinje cells (Dittmann et al., 2000), stellate cells (Carter and Regehr, 2000) and Golgi cells (Bureau et al., 2000; Watanabe and Nakanishi, 2003).

Conclusions and functional implications

Regulation of response initiation by changes in release probability is suitable to perform the extensive spatio-temporal recoding of mossy fiber inputs predicted by certain cerebellar theories (Braitenberg, 1967; Medina and Mauk, 2000; DeSchutter and Bjaalie, 2001). For example, setting the appropriate delay in granule cell responses could be critical for eye-blink reflex conditioning. Interestingly, timing of conditioned stimuli carried by mossy fibers is learned with millisecond precision in the time range (<150 ms) characteristic of LTP-dependent delay regulation (Hansel et al., 2001; Koekkoek et al., 2002). Other mechanisms, like regulation of granule cell intrinsic excitability or yet undiscovered changes in postsynaptic conductance, could be important to control the gain of the mossy fiber input along specific input lines (Albus, 1971; Silver, 2003), modulating the frequency of Purkinje cell discharge as in the VOR (van Alphen and De Zeeuw, 2002). Implementation of large-scale cerebellar network simulations may be useful to further clarify the computational implications of short- and long-term synaptic plasticity at the mossy fiber – granule cell relay of cerebellum.

REFERENCES

1. Albus JS. A theory of cerebellar function. *Math Biosc* 10:25-61, 1967.
2. Armano S, Rossi P, Taglietti V, and D'Angelo E. Long-term potentiation of intrinsic excitability at the mossy fiber-granule cell synapse of rat cerebellum. *J Neurosci* 20:5208-5216, 2000.

3. Barbour B. An evaluation of synapse independence. *J Neurosci* 21:7969-7984, 2001.
4. Bliss TV, Collingridge GL and Morris RG. Long-term potentiation and structure of the issue. Philos Trans R Soc Lond B Biol Sci. 358:607-611, 2003.
5. Braitenberg V. Is the cerebellar cortex a biological clock in the millisecond range? *Prog Brain Res* 25:334-346, 1967.
6. Brenowitz S, and Trussell LO. Minimizing synaptic depression by control of release probability. *J Neurosci* 21:1857-1867, 2001.
7. Buonomano DV. Decoding temporal information: A model based on short-term synaptic plasticity. *J Neurosci* 20:1129-1141, 2000.
8. Bureau I, Dieudonne S, Coussen F, and Mulle C. Kainate receptor-mediated synaptic currents in cerebellar Golgi cells are not shaped by diffusion of glutamate. *Proc Natl Acad Sci USA* 97: 6838-6843, 2000.
9. Carey M, and Lisberger S. Embarrassed, but not depressed: eye opening lessons for cerebellar learning. *Neuron* 35:223-226, 2002.
10. Carter AG, and Regehr WG. Prolonged synaptic currents and glutamate spillover at the parallel fiber to stellate cell synapse. *J Neurosci* 20:4423-4434, 2000.
11. Casado M, Isope P, and Ascher P. Involvement of presynaptic N-methyl-D-aspartate receptors in cerebellar long-term depression. *Neuron* 33:123-130, 2002.
12. Cathala L, Brickley S, Cull-Candy S, and Farrant M. Maturation of EPSCs and intrinsic membrane properties enhances precision at a cerebellar synapse. *J Neurosci* 23:6074-6085, 2003.
13. Chadderton P, Margrie TW, and Häusser M. Integration of quanta in cerebellar granule cells during sensory processing. *Nature* 428:856-860, 2004.
14. Coesmans M, Weber JT, De Zeeuw CI, and Hansel C. Bidirectional Parallel Fiber Plasticity in the Cerebellum under Climbing Fiber Control. Neuron 44:691-700, 2004.
15. Crank J. The Mathematics of Diffusion Publications, Oxford Science (ed.), 1975.
16. D'Angelo E, De Filippi G, Rossi P, and Taglietti V. Synaptic excitation of individual rat cerebellar granule cells in situ: evidence for the role of NMDA receptors. *J Physiol* 484:397-413, 1994.
17. D'Angelo E, Nieus T, Maffei A, Armano S, Rossi P, Taglietti V, Fontana A, and Naldi G. Theta-frequency bursting and resonance in cerebellar granule cells: experimental evidence and modeling of a slow K^+-dependent mechanism. *J Neurosci* 21: 759-770, 2001.

18. D'Angelo E, Rossi P, Armano S, and Taglietti V. Evidence for NMDA and mGlu receptor-dependent long-term potentiation of mossy fiber-granule cell transmission in rat cerebellum. *J Neurophysiol* 81:277-287, 1999.
19. D'Angelo E, Rossi P, and Taglietti V. Voltage-dependent kinetics of N-methyl-D-aspartate synaptic currents in rat cerebellar granule cells. Eur J Neurosci 6:640-645, 1994.
20. Debanne D, Daoudal G, Sourdet V, Russier M. Brain plasticity and ion channels. *J Physiol (Paris)* 97:403-414, 2003.
21. De Schutter E, and Bjaalie JG. Coding in the granular layer of the cerebellum. *Prog Brain Res* 130:279-296, 2001.
22. Destexhe A, Mainen ZF, and Sejnowski TJ. Synthesis of models for excitable membranes, synaptic transmission and neuromodulation using a common kinetic formalism. *J Comput Neurosci* 1:195-230, 1994.
23. Diamond JS and Jahr CE. Transporters buffer synaptically released glutamate on a submillisecond time scale. J Neurosci 17:4672-87, 1997.
24. DiGregorio DA, Nusser Z and Silver RA. Spillover of glutamate onto synaptic AMPA receptors enhances fast transmission at a cerebellar synapse. *Neuron* 35:521-533, 2002.
25. Dittman JS, Kreitzer AC, and Regehr WG. Interplay between facilitation, depression, and residual calcium at three presynaptic terminals. *J Neurosci* 20:1374-1385, 2000.
26. Dodge FA, and Rahamimoff R. Co-operative action a calcium ions in transmitter release at the neuromuscular junction. *J Physiol* 193:419-432, 1967.
27. Eccles JC, Ito M, and Szentagothai J. The cerebellum as a neuronal machine Berlin, Springer (ed.) , 1967.
28. Gall D, Prestori F, Sola E, D'Errico A, Roussel C, Forti F, Rossi P, and D'Angelo E. Intracellular calcium regulation by burst discharge determines bidirectional long-term synaptic plasticity at the cerebellum input stage. J Neurosci 25:4813-4822, 2005.
29. Gupta A, Wang Y, and Markram H. Organizing principles for a diversity of GABAergic interneurons and synapses in the neocortex. *Science* 287:273-278, 2000.
30. Han VZ, Grant K, and Bell CC. Reversible associative depression and nonassociative potentiation at a parallel fiber synapse. *Neuron* 27:611-622, 2000.
31. Hansel C, Linden DJ, and D'Angelo E. Beyond parallel fiber LTD: the diversity of synaptic and non-synaptic plasticity in the cerebellum. *Nat Neurosci* 4:467-475, 2001.
32. Hines ML, and Carnevale NT. NEURON: a tool for neuroscientists. *Neuroscientist* 7:123-135, 2001.

33. Jakab RL, and Hámori J. Quantitative morphology and synaptology of cerebellar glomeruli in the rat. *Anat Embryol (Berl)* 179:81-88, 1988.
34. Kase M, Miller DC, and Noda H. Discharges of Purkinje cells and mossy fibres in the cerebellar vermis of the monkey during saccadic eye movements and fixation. *J Physiol* 300:539-555, 1980.
35. Katz B, and Miledi R. The role of calcium in neuromuscular facilitation. *J Physiol* 195:481-492, 1968.
36. Koekkoek SK, Den Ouden WL, Perry G, Highstein SM, and De Zeeuw CI. Monitoring kinetic and frequency-domain properties of eyelid responses in mice with magnetic distance measurement technique. *J Neurophysiol* 88: 2124-2133, 2002.
37. Krahe R, and Gabbiani F. Burst firing in sensory systems. *Nat Rev Neurosci* 5:13-23, 2004.
38. Kullmann DM, Erdemli G, and Asztély F. LTP of AMPA and NMDA receptor-mediated signals: evidence for presynaptic expression and extrasynaptic glutamate spill-over. *Neuron,*17: 461-474, 1996.
39. Lisman JE. Bursts as a unit of neural information: making unreliable synapses reliable. *Trends Neurosci* 20:38-43, 1997.
40. Lisman JE. Long-term potentiation: outstanding questions and attempted synthesis. Philos Trans R Soc Lond B Biol Sci. 358:829-842, 2003.
41. Maffei A, Prestori F, Shibuki K, Rossi P, Taglietti V, and D'Angelo E. NO enhances presynaptic currents during cerebellar mossy fiber-granule cell LTP. J Neurophysiol 90:2478-2483, 2003.
42. Mainen ZF, Malinow R and Svoboda K. Synaptic calcium transients in single spines indicate that NMDA receptors are not saturated. *Nature* 399:151-155, 1999.
43. Malenka RC, and Nicoll RA. Long-term potentiation - A decade of progress? *Science* 285:1870-1874, 1999.
44. McAllister AK, and Stevens CF. Nonsaturation of AMPA and NMDA receptors at hippocampal synapses. *Proc Natl Acad Sci USA* 97:6173-6178, 2000.
45. Medina JF, and Mauk MD. Computer simulation of cerebellar information processing. *Nat Neurosci Rev 3*:1205-1211, 2000.
46. Mitchell SJ, and Silver RA. Shunting inhibition modulates neuronal gain during synaptic excitation. *Neuron* 38:433-445, 2003.
47. Neher E, and Sakaba T. Estimating transmitter release rates from postsynaptic current fluctuations. *J. Neurosci.* 21:9638-9654, 2001.

48. Nielsen TA, DiGregorio DA, and Silver RA. Modulation of Glutamate Mobility Reveals the Mechanism Underlying Slow-Rising AMPAR EPSCs and the Diffusion Coefficient in the Synaptic Cleft. *Neuron* 42:757-771, 2004.
49. O'Donovan MJ, and Rinzel J. Synaptic depression: a dynamic regulator of synaptic communication with varied functional roles. *Trends Neurosci* 20:431-433, 1997.
50. Overstreet LS, Kinney GA, Liu Y-B, Billups D, and Slater NT. Glutamate transporters contribute to the time course of synaptic transmission and plasticity at a cerebellar synapse. *J Neurosci* 22:9687-9697, 2002.
51. Raman I, and Trussell L. The mechanism of alpha-amino-3-hydroxy-5-methyl-4-isoxazolepropionate receptor desensitization after removal of glutamate. *Biophys J*. 68:137-146, 1995.
52. Rieke F, Warland D, Steveninck R, and Bialek W. Spikes : Exploring the neural code *The MIT Press, Cambridge MA 1996.*
53. Rosenmund C, Feltz A, and Westbrook GL. Synaptic NMDA receptor channels have a low open probability. *J Neurosci* 15:2788-2795, 1995.
54. Rossi P, Sola E, Taglietti V, Borchardt T, Steigerwald F, Utvik JK, Ottersen OP, Köhr G, and D'Angelo E. NMDA receptor 2 (NR2) C-terminal control of NR open probability regulates synaptic transmission and plasticity at a cerebellar synapse. *J Neurosci* 22:9687-9697, 2002.
55. Saftenku EE. Modeling of slow glutamate diffusion and AMPA receptor activation in the cerebellar glomerulus. J Theor Biol 234:363-382, 2005.
56. Selig DK, Nicoll RA, Malenka RC. Hippocampal long-term potentiation preserves the fidelity of postsynaptic responses to presynaptic bursts. J Neurosci. 19:1236-1246, 1999.
57. Silver RA, Colquhoun D, Cull-Candy SG, and Edmonds B. Deactivation and desensitization of non-NMDA receptors in patches and the time course of EPSCs in rat cerebellar granule cells. *J Physiol* 493:167-173, 1996a.
58. Silver RA, Cull-Candy SG, and Takahashi T. Non-NMDA glutamate receptor occupancy and open probability at a rat cerebellar synapse with single and multiple release sites. *J Physiol* 494:231-250, 1996b.
59. Sola E, Prestori F, Rossi P, Taglietti V, and D'Angelo E. Increased neurotransmitter release during long-term potentiation at mossy fibre-granule cell synapses in rat cerebellum. *J Physiol* 557: 843-861, 2004.
60. Traynelis SF, Silver RA, and Cull-Candy SG. Estimated conductance of glutamate receptor channels activated during EPSCs at the cerebellar mossy fiber-granule cell synapse. *Neuron* 11:279-289, 1993.

61. Tsodyks MV, and Markram H. The neural code between neocortical pyramidal neurons depends on neurotransmitter release probability. *Proc Natl Acad Sci USA* 94:719-723, 1997.
62. Tsodyks M, Uziel A, and Markram H. Synchrony generation in recurrent networks with frequency-dependent synapses. J Neurosci 20: RC50, 2000.
63. van Alphen AM, and De Zeeuw CI. Cerebellar LTD facilitates but is not essential for long-term adaptation of the vestibulo-ocular reflex. *Eur J Neurosci* 16:486-490, 2002.
64. Wadiche J, and Jahr C. Multivesicular release at climbing fiber-Purkinje cell synapses. Neuron 32:301-13, 2001.
65. Wang SS, Denk W, and Häusser M. Coincidence detection in single dendritic spines mediated by calcium release. *Nat Neurosci* 3:1266-1273, 2000.
66. Watanabe D, and Nakanishi S. mGluR2 postsynaptically senses granule cell inputs at Golgi cell synapses. *Neuron* 39:821-829, 2003.
67. Xu-Friedman MA, Regehr WG. Ultrastructural contributions to desensitization at cerebellar mossy fiber to granule cell synapses. *J Neurosci* 23:2182-2192, 2003.

TABLES

Table 1. Neurotransmission parameters obtained from fitting of EPSC trains. Values represent the average of measurements obtained in different cells (n=7 for regular 100 Hz trains; n=4 for random Poisson trains with 50 Hz mean frequency). Note that parameters obtained from fittings in regular and random trains are not statistically different.

	Regular train	Random train	p (unpaired *t*-test)
p	0.42±0.05	0.36±0.07	0.71
τ_F (ms)	10.8±0.8	39.4±17.5	0.21
τ_R (ms)	35.1±3.6	16.5±4.5	0.09
τ_I (ms) *	1	1	* fixed
r (μm)	1.03±0.10	0.92±0.12	0.69
M (molecules)	21514.6±3156.8	31688.1±7403.1	0.36
D_{eff} ($\mu m^2 ms^{-1}$)	0.22±0.03	0.12±0.01	0.19

FIGURE 1

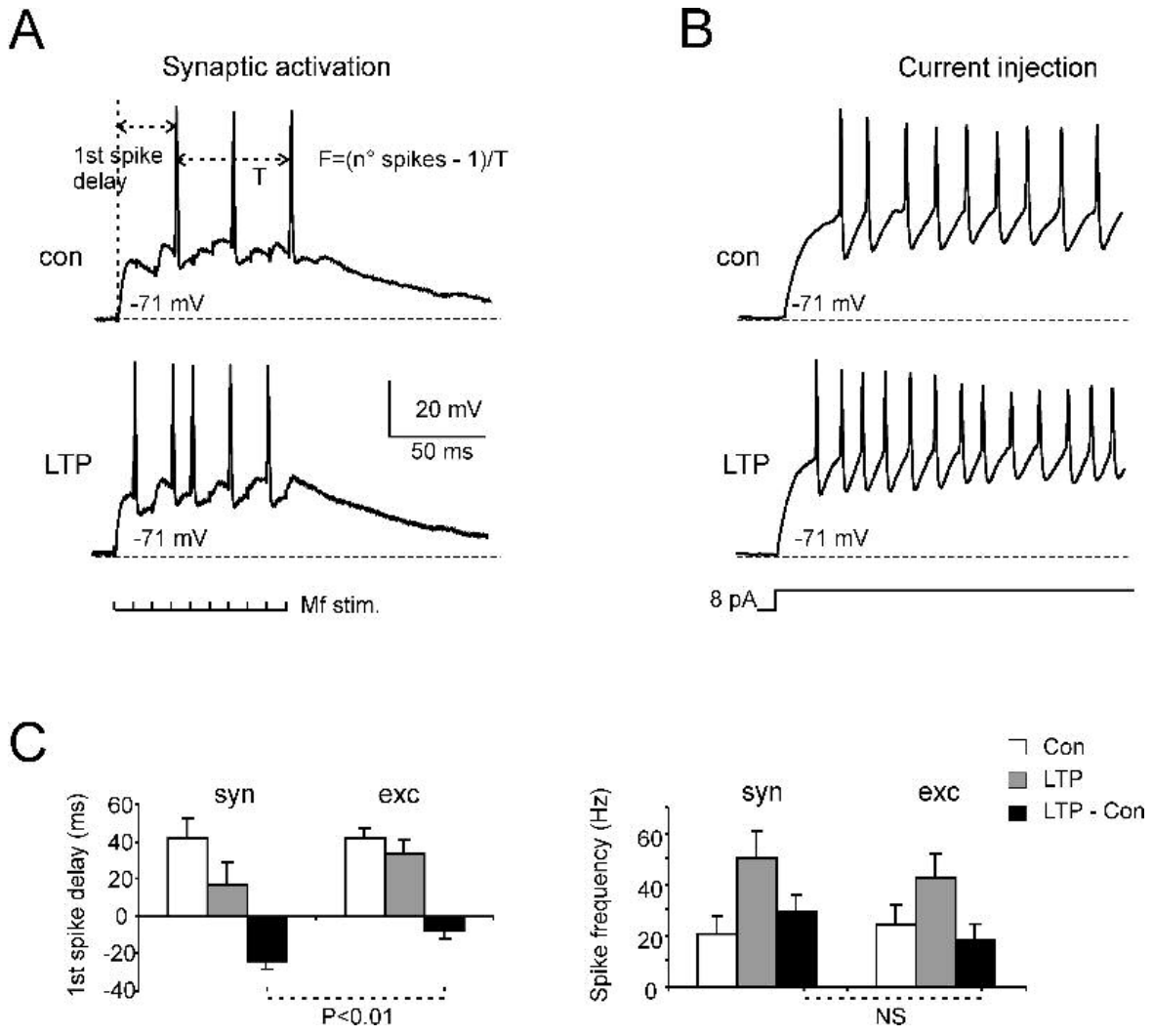

Fig. 1. *The effect of LTP on granule cell firing during repetitive neurotransmission.* (A) Mossy fibers are stimulated with a 100 Hz – 100 ms train determining EPSP temporal summation and spike activation in a granule cell. Twenty minutes after LTP induction, mossy fiber stimulation elicits spikes with shorter delay and higher frequency. Labels and arrows indicate the first spike delay and how the mean discharge frequency F is calculated from the number of interspike intervals and the burst duration. (B) In the same cell, a depolarizing current step is injected to test intrinsic electroresponsiveness. (C) The histogram demonstrates that shortening in first-spike delay is more prominent during synaptic stimulation (syn) than during injection of current pulses (exc). Shortening in first-spike delay is statistically significant ($p<0.01$, $n=7$). No significant difference is observed concerning firing frequency (NS, $n=7$)

FIGURE 2

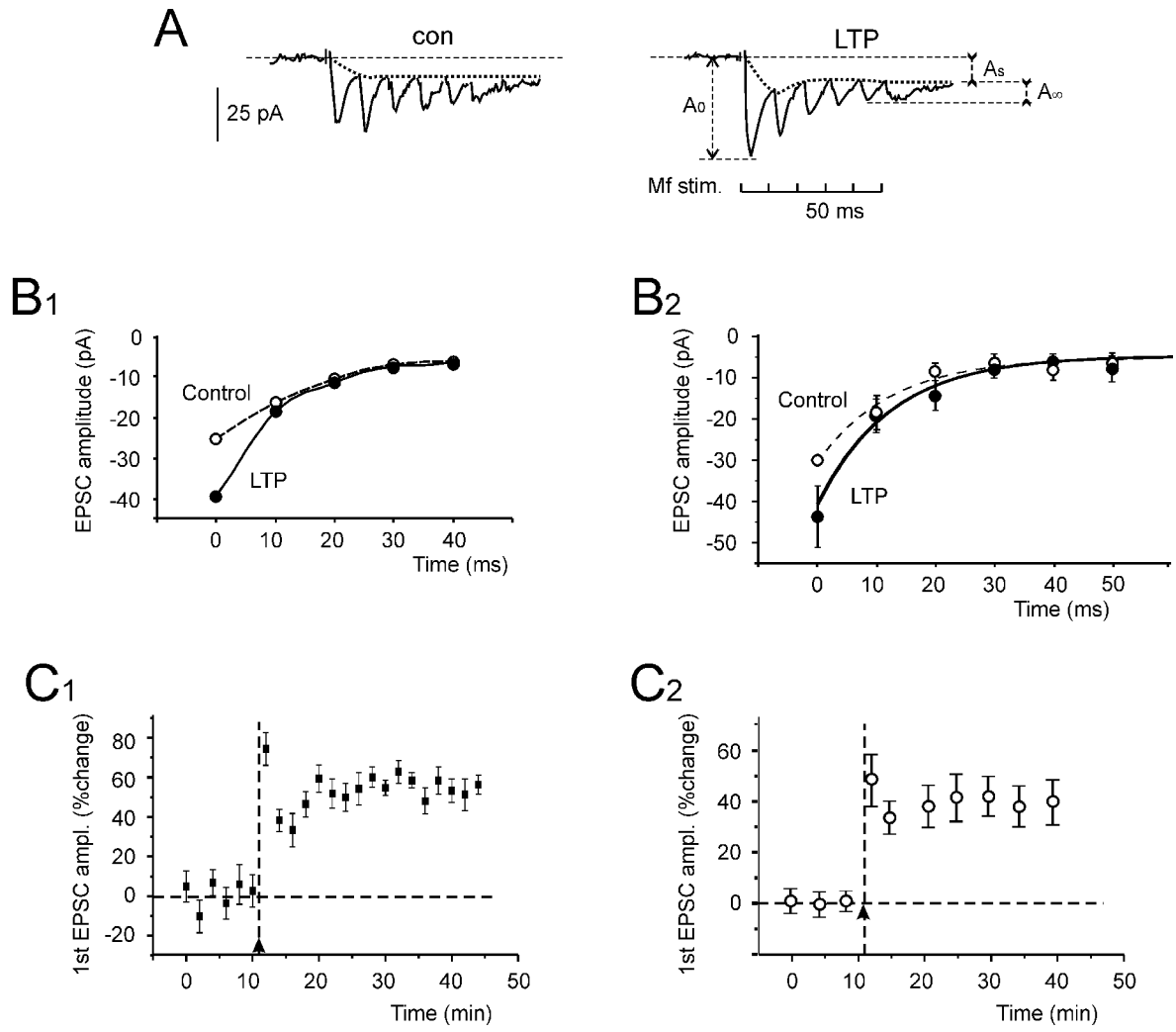

Fig. 2. *The effect of LTP on granule cell EPSCs during repetitive neurotransmission.* An example of LTP experiment using short stimulus bursts. LTP was induced by TBS during depolarization at –40 mV. EPSCs were recorded at –70 mV. (A) EPSCs generated with a 100 Hz – 50 ms train show stronger short-term depression following LTP induction. Note that the sustained current (dotted lines) determined by spillover also increases during LTP. The measures taken from EPSC trains are indicated: 1st EPSC amplitude A_0, steady-state EPSC amplitude A_∞, sustained baseline current A_s. EPSC amplitude is measured at peak relative to the baseline current immediately preceding the response. (B_1) The time course of EPSC amplitude in control (○) and during LTP (●) for the EPSC trains shown in A. (B_2) Average time course of EPSC amplitude (n=8; mean ±SEM, n=10). Data points are interpolated with exponential fits, whose parameters are reported in the text. Note the different decay rate but similar steady-state amplitude (A_∞) level attained at the end of the EPSC trains. (C_1) Time course of LTP evaluated on the 1st EPSC in the trains. Data points are taken from the average of subsequent sweeps (mean ±SEM, n=10) in the same cell as in A and B_1. (C_2) Average time course of LTP profile (n=8; mean ±SEM). LTP is induced by TBS at the arrowhead. Note that a brief post-tetanic potentiation or STP is followed by persistent potentiation.

FIGURE 3

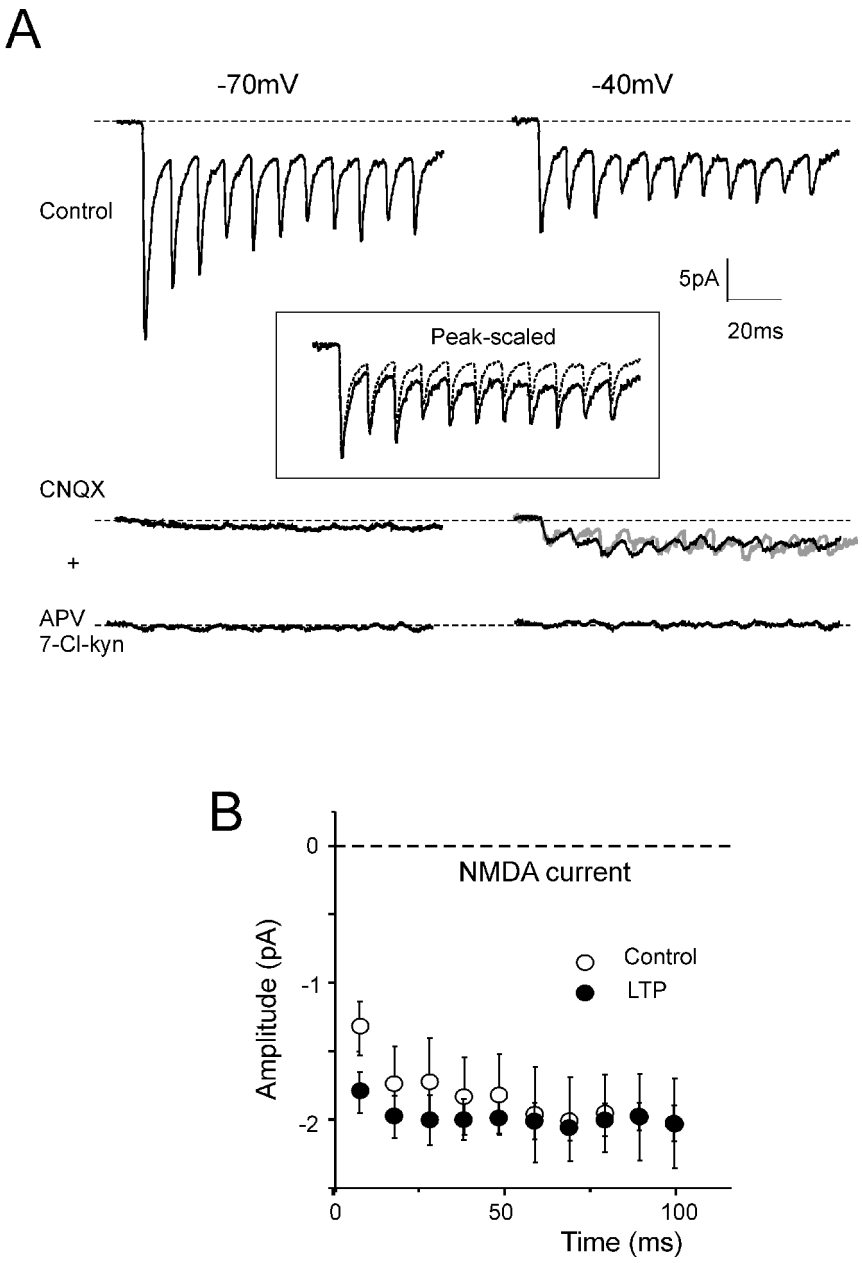

Fig. 3. *NMDA currents in EPSC trains.* (A) The NMDA current was recorded in 100 Hz trains both at –70 mV and at –40 mV in control solution, after application of 10 μM CNQX, and after addition of 100 μM APV and 50 μM 7Cl-Kyn. Each trace is the average of 20 sweeps. Note the large sustained component at –40 mV (top right), its dependence from the NMDA current (middle right), the negligible NMDA current isolated at –70 mV (middle left), and the complete block of currents by ionotropic receptor antagonists (bottom). The inset shows the peak-scaled EPSC train at –70 mV (dashed trace) superimposed over that at –40 mV (full trace). In the middle right panel, the NMDA current obtained by digital subtraction of peak-scaled EPSC trains (gray trace) is superimposed over that obtained pharmacologically (black trace). The NMDA current obtained by digital and pharmacological subtraction coincide and account for a large part of the sustained current at –40 mV. (B) Experimental points (mean±SEM; n=20) show NMDA currents obtained with minimal stimulation after subtraction of AMPA currents in control (○) and during LTP (●).

FIGURE 4

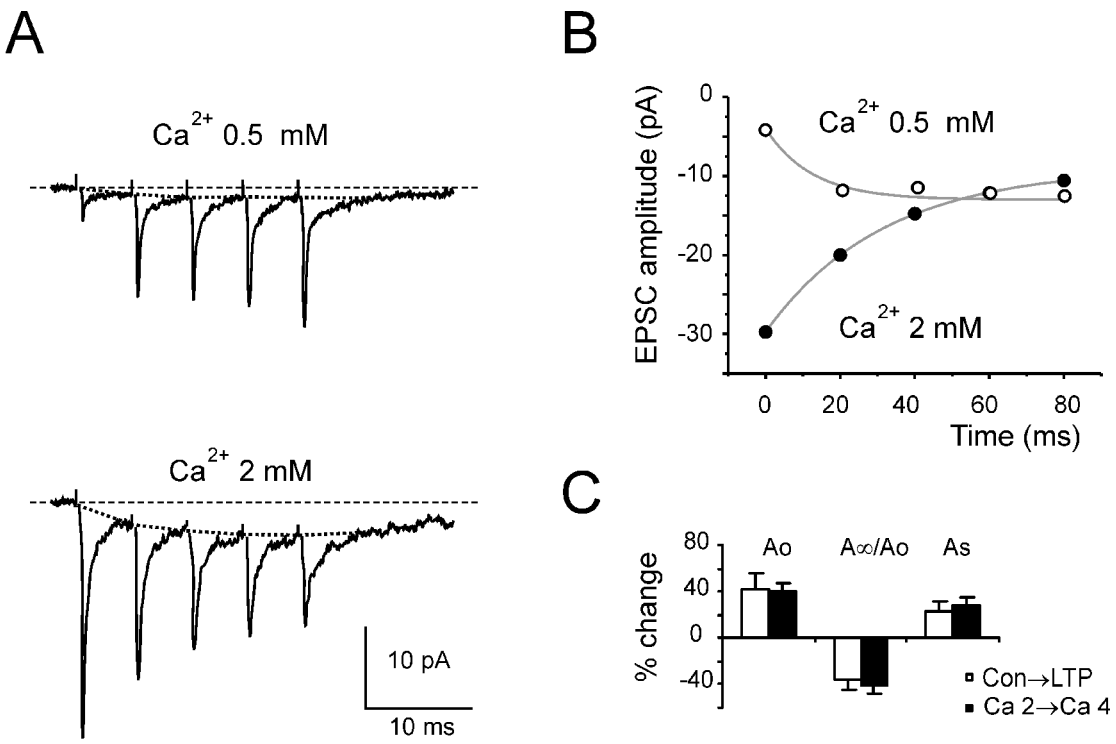

Fig. 4. *Ca^{2+}-dependence of short-term plasticity in EPSC trains*. (A) The traces show AMPA EPSC trains elicited in low and normal Ca^{2+} concentration at 50 Hz. EPSC facilitation in low Ca^{2+} is converted into depression in normal Ca^{2+}. Note the increased baseline current (dotted line) in 2 mM Ca^{2+}. (B) Time course of EPSC amplitude in the same experiments shown in A with exponential fits superimposed. Facilitation is converted into depression by changing from 0.5 mM to 2 mM Ca^{2+}. Each trace is the average of 50 sweeps. (C) The histogram shows the percent change in A_0, A_∞/A_0 , and A_s when Ca^{2+} is increased from 2 mM to 4 mM. Note the similarity with changes elicited by LTP in the same parameters.

FIGURE 5

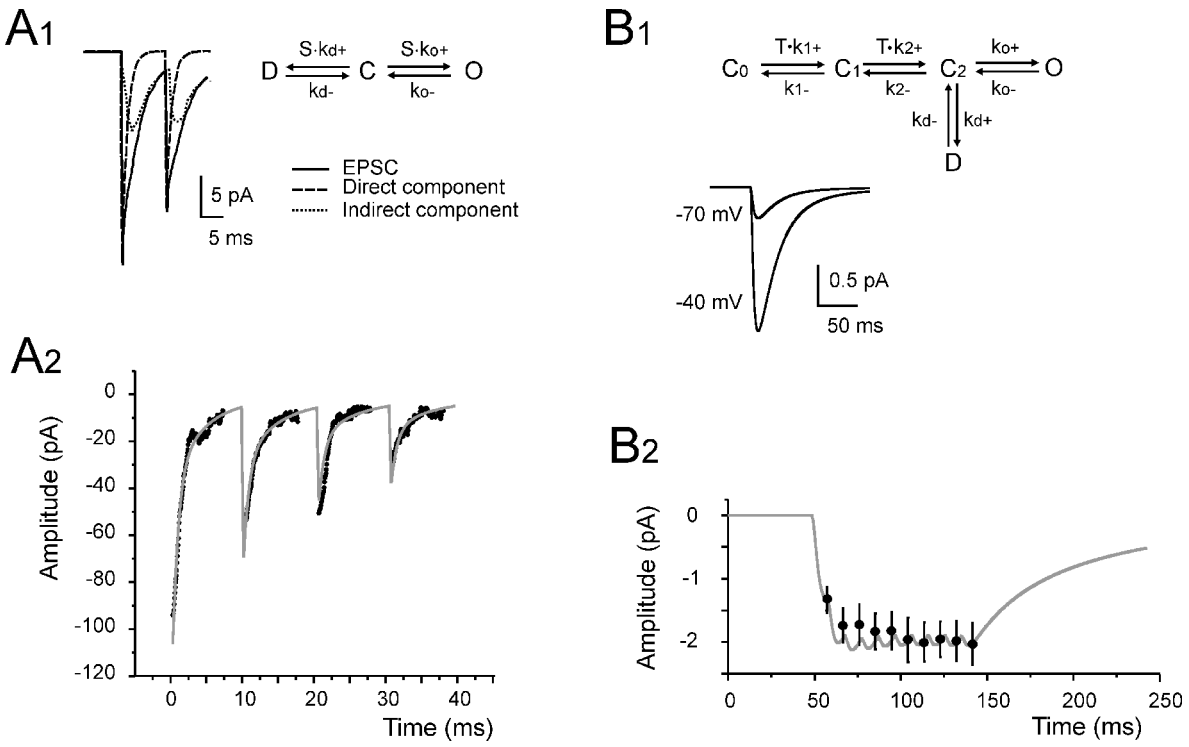

Fig. 5. *Mathematical modeling of repetitive neurotransmission.* **(A_1)** The simulated AMPA current is composed of a fast *direct* response and a slow *indirect* response caused by spillover. Spillover generates a sizeable tonic current and slows down EPSC decay. The kinetic scheme is shown at the top. **(A_2)** The model (gray line) was used to fit a regular AMPA EPSC train (100 Hz). EPSCs were measured at –70 mV in the presence of 100 μM APV and 50 μM 7Cl-Kyn to suppress the NMDA current. 50 traces were averaged to suppress stochastic variability. Fitting was performed in two steps. First, we fitted the first EPSC in the train obtaining D_{eff}= 0.41μm^{2}ms^{-1}, r=1.91 μm, M=27365. Secondly, after fixing these parameters, the whole EPSC train was fitted obtaining p=0.49, τ_R=53.8 ms, τ_F =10.0 ms. **(B_1)** The simulated NMDA current is much slower than the AMPA and is fully generated by spillover. The kinetic scheme is shown at the top. **(B_2)** The NMDA current model (continuous line), which was obtained using p=0.4, follows the experimental points (replotted from Fig. 3B).

FIGURE 6

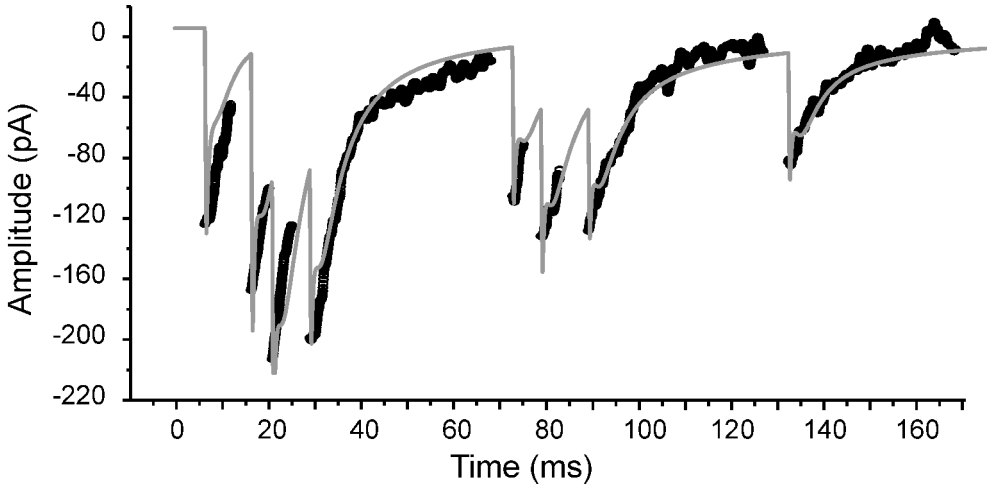

Fig. 6. *Fitting of the model to random EPSC trains*. The model (gray line) was used to fit a random EPSC train (50 Hz mean frequency, Poisson distribution) obtained by averaging 50 sweeps to suppress stochastic variability.

FIGURE 7

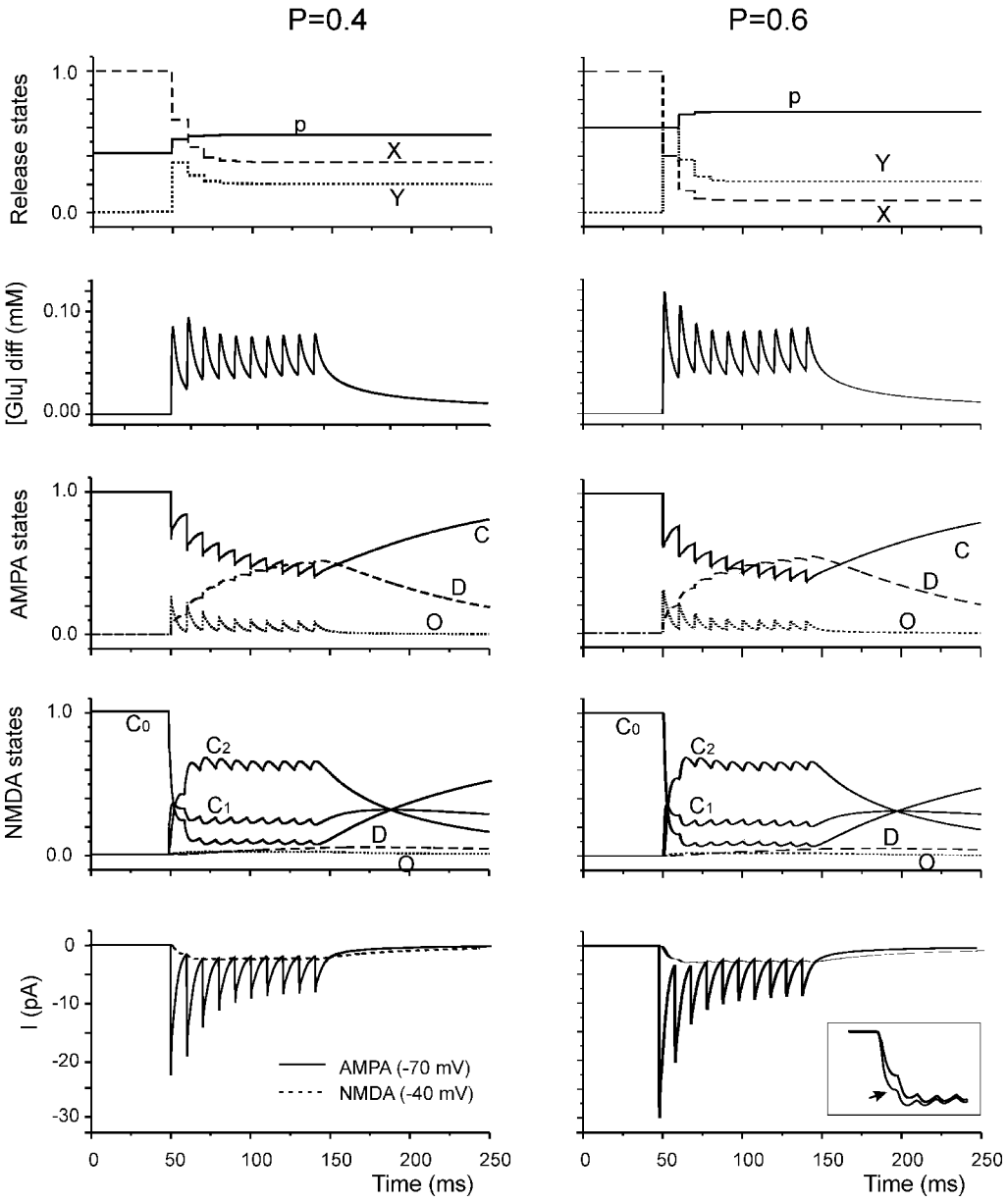

Fig. 7. *Pre- and postsynaptic mechanisms in EPSC trains.* The plot shows model parameters during 100 Hz stimulation at p=0.4 (left) and p=0.6 (right). With this initial p value, the reserve pool X decrease during the train (depletion) prevails over use-dependent P increase (facilitation) causing a net depression of available resource Y (the apparent lack of recovery in X, Y and p is due to discontinuous calculation of the parameters, which occurs only when a pulse arrives; see Methods). Glutamate spillover increases due to slow temporal summation of diffusive waves. Glutamate binding to AMPA receptors moderately reduces C remaining far from saturation, desensitization D increases, and opening O decreases toward steady-state in a few responses. Glutamate binding to NMDA receptors strongly reduces C_0 approaching saturation (while glutamate could still bind to C_1), opening O maintains low levels because of low channel open probability, and desensitization D slowly increases. The corresponding AMPA and NMDA currents are plotted at the bottom. The NMDA currents are enlarged and super-imposed in the inset.

FIGURE 8

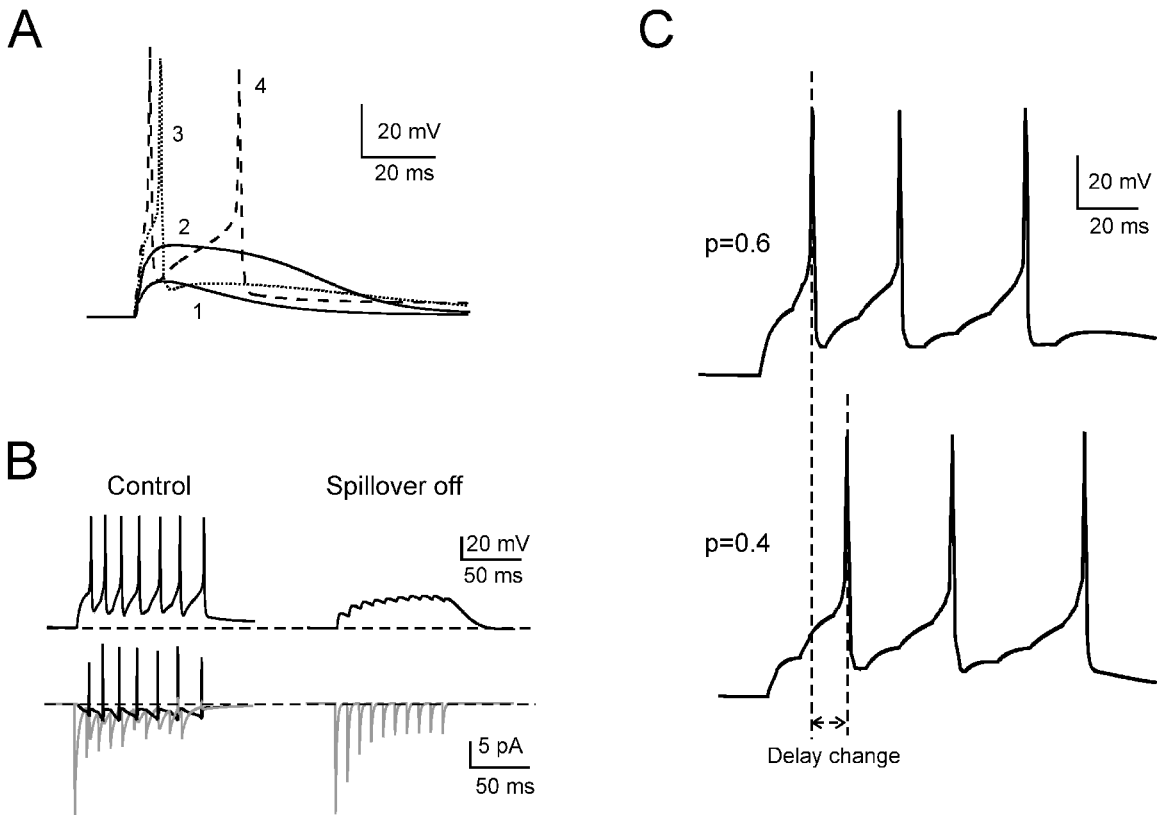

Fig. 8. *Simulation of synaptic excitation and LTP.* (A) The model reproduced activation of EPSPs and EPSP-spike complexes by 1, 2, 3 (dotted trace), or 4 (dashed trace) mossy fibers as in D'Angelo et al. (1995). Note that the single fiber EPSP measured 14 pA, peaked in 8 ms and lasted 27 ms at half-peak amplitude, very close to experimental estimates. (B) Response to spike trains at 100 Hz with 2 simultaneously active mossy fibers. Firing was depressed by switching off glutamate spillover currents. Note strong depression in AMPA EPSCs. Lower traces show the corresponding AMPA (gray) and NMDA (black) currents. (C) Regulation of EPSP temporal summation by a change in *p* from 0.4 to 0.6 simulating LTP. Note the shorter 1st spike delay at *p*=0.6.

FIGURE 9

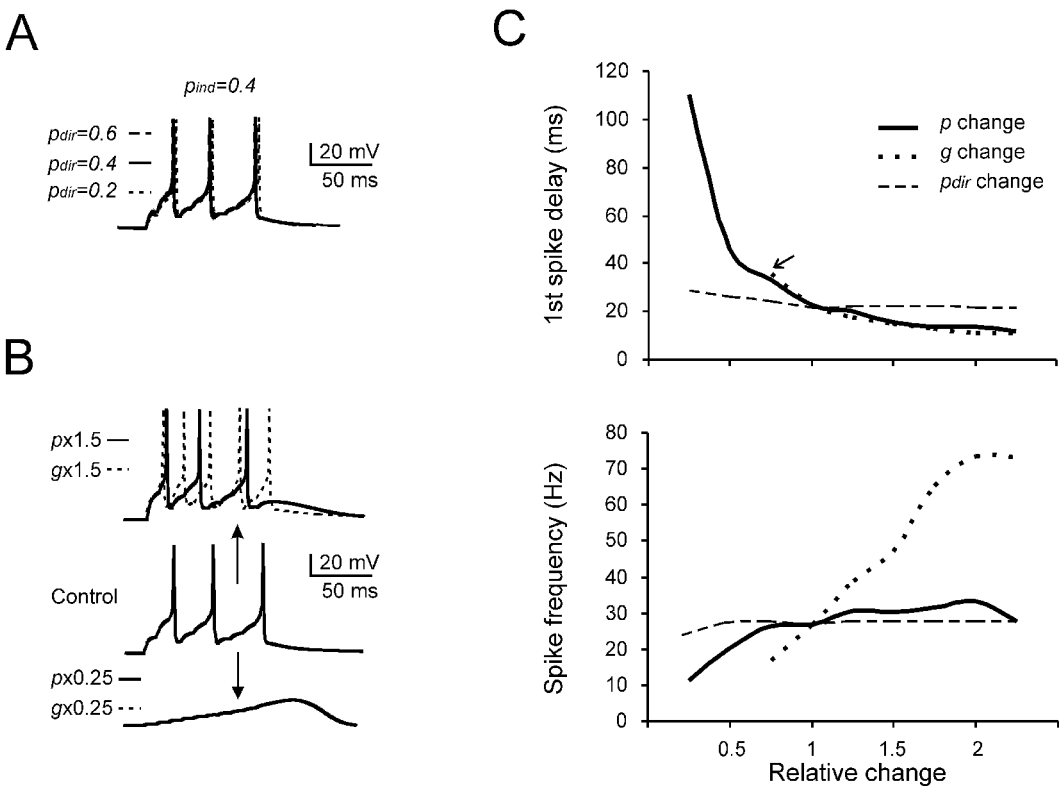

Fig. 9. *Simulation of alternative potentiation models.* (A) When spillover is left unchanged (p_{ind}=0.4) and only direct release is changed by 0.25-times or 1.5-times (p_{dir}=0.2, 0.4, 0.6), no remarkable modulation in granule cell discharge is observed. (B) The effect of changing release probability or maximum conductance are compared. Starting from p=0.4, p was either increased by 1.5 times or decreased by 0.25 times. The results are compared with corresponding changes in maximum conductance, g. (C) Dependence of first spike delay and average discharge frequency on release probability and postsynaptic conductance. The curves correspond to activation of 1 mossy fiber. Note that, unlike p, g has a limited control on delay (beginning at the arrow) but a strong influence on firing frequency. A change in p_{dir} causes poor modulation in either delay or frequency.

FIGURE 10

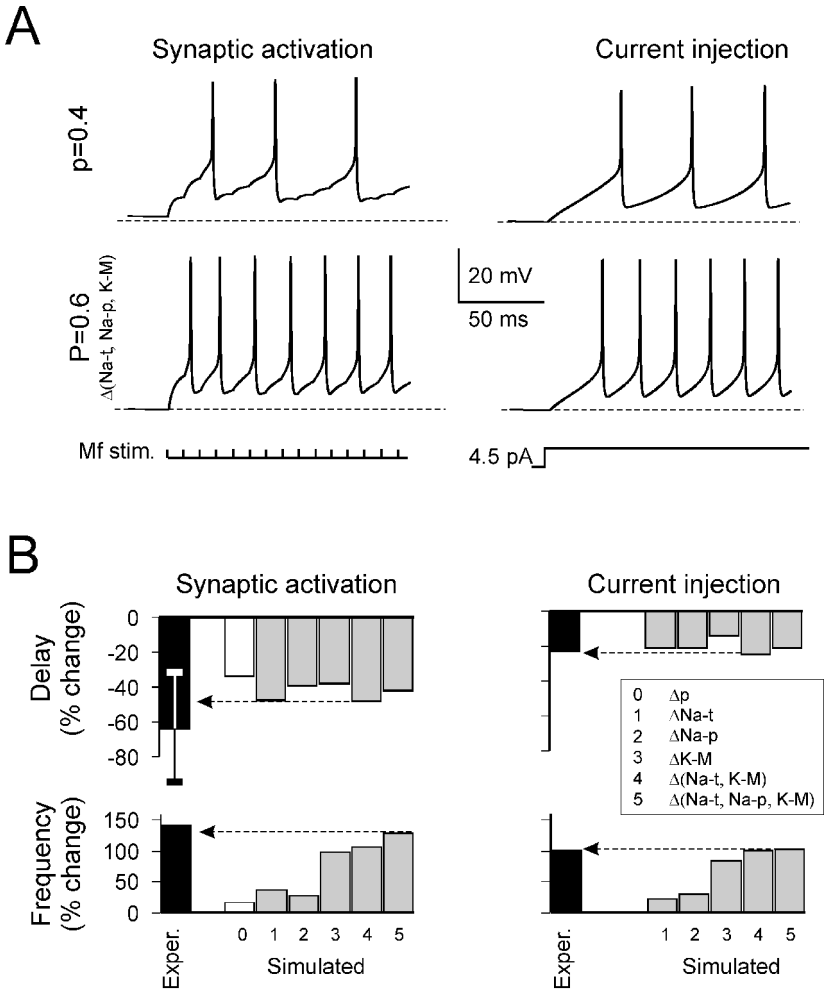

Fig. 10. *Simulation of changes in intrinsic excitability.* (A) Action potential firing was simulated by either 100 Hz stimulation of a single synapse or by depolarizing current injection from –71.5 mV (the mean holding potential of experiments reported in Fig. 1C). LTP was simulated by raising *p* and by changing postsynaptic currents ($I_{K\text{-}M}$, $I_{Na\text{-}t}$, $I_{Na\text{-}p}$), as explained in B. (B) Simulations of the changes in first-spike delay and firing frequency associated with LTP are compared to those observed experimentally. The experimental changes have been obtained from data reported in Fig. 1C. Synaptic transmission was potentiated by raising *p* from 0.4. to 0.6, and intrinsic excitability was enhanced by reducing $I_{K\text{-}M}$ (x 0.12), raising $I_{Na\text{-}p}$ (x 1.5), and lowering $I_{Na\text{-}t}$ activation (–3mV). The changes in postsynaptic currents were also combined, as indicated. The combination $\Delta(I_{K\text{-}M}, I_{Na\text{-}t}, I_{Na\text{-}p})$ proved very effective in reproducing changes in intrinsic excitability and was therefore adopted to simulate responses to 100 Hz synaptic stimulation. During synaptic stimulation, the first-spike delay and firing frequency increase observed during LTP were reproduced within the experimental error (±SEM bars are shown only for delay changes during synaptic simulation). The dashed arrows facilitate the comparison of simulated with experimental results. It should be noted that release probability is very effective in regulating delay but poorly effective in regulating firing frequency.